JOURNAL OF GUIDANCE, CONTROL, AND DYNAMICS
Vol. 32, No. 3, May–June 2009

Solar Sail Dynamics and Coning Control in Circular Orbits

Dale A. Lawrence*
University of Colorado, Boulder, Colorado 80309
and
Mark S. Whorton†
Teledyne Brown Engineering, Inc., Huntsville, Alabama 35805

DOI: 10.2514/1.35970

Attitude dynamics of a solar sail are described relative to an orbiting local-vertical/local-horizontal frame under the influence of aerodynamic, solar, and gravity-gradient torques. The complete set of equilibria of the sail normal vector in local-vertical/local-horizontal is described as a function of sailcraft spin rate and orbit and sailcraft design parameters. These equilibria enable orbit-rate coning of the sail normal that is useful for changing orbit parameters using solar thrust. Lyapunov stability properties of the equilibria are analyzed, providing conditions for stable equilibria. Feedback control is considered for stabilization and additional damping, enabling any of the equilibria to be asymptotically stabilized. This approach enables long-term thrust-vector control in the presence of large environmental torques for significant orbit-parameter variation over time. An example of a 3 kg microsailcraft is used to illustrate the equilibrium and stability conditions and the performance of the attitude control.

Nomenclature

A	=	planet-centered inertial frame ($\hat{x}$, $\hat{y}$, and $\hat{z}$)
A_s	=	sail area, m^2
a	=	orbit semimajor axis, m
B	=	intermediate sailcraft-centered frame ($\hat{l}$, $\hat{m}$, and $\hat{n}$)
C	=	sailcraft body-fixed frame ($\hat{p}$, $\hat{q}$, and $\hat{n}$)
C_D	=	ballistic coefficient of drag
f_s	=	specular reflectance fraction
${}^A\mathbf{h}_C$	=	inertial angular momentum vector of C about the sailcraft center of mass, N · m · s
$\mathbf{I}$	=	identity tensor
I_n	=	principal sailcraft moment of inertia about sail normal, kg · m^2
$\mathbf{I}_s$	=	sailcraft moment-of-inertia tensor about the sailcraft center of mass, kg · m^2
I_T	=	principal sailcraft moment-of-inertia transverse to sail normal, kg · m^2
L	=	local-vertical/local-horizontal orbit frame ($\hat{r}$, $\hat{v}$, and $\hat{o}$)
$\hat{n}$, $\hat{n}_o$	=	sail normal unit vector, nominal equilibrium normal vector
P	=	solar pressure, N/m^2
r_c	=	sailcraft c.p.–c.m. offset, m
$\hat{s}$	=	sailcraft-to-sun unit vector
V_1, V_2, V_3, V_a, V_b	=	Lyapunov function components
v	=	sailcraft velocity relative to the atmosphere, m/s
β	=	cone half-angle of the sail normal $\hat{n}$ in L, rad
δ_n	=	vector of deviations of $\hat{n}$ orthogonal to $\hat{n}_0$
μ	=	planetary gravitational constant, m^3/s^2
ρ	=	atmospheric density, kg/m^3
τ_{am}, τ_{sm}, τ_{gm}	=	positive moment coefficients due to aerodynamic, solar, and gravity-gradient torques, N · m
ϕ	=	clock angle of the sail normal $\hat{n}$ in L, rad
Ψ_a, Ψ_s, Ψ_g	=	aerodynamic, solar, and gravity-gradient potentials, N · m/rad
ω_n	=	component of ${}^A\boldsymbol{\omega}_C$ along the sail normal $\hat{n}$, rad/s
ω_{no}	=	equilibrium value of ω_n, rad/s
ω_T	=	component of ${}^A\boldsymbol{\omega}_B$ orthogonal to $\hat{n}$, rad/s
ω_o	=	orbit angular velocity, rad/s
$\omega_\perp$	=	component of ${}^A\boldsymbol{\omega}_L$ along $\hat{n}$, rad/s
${}^A\boldsymbol{\omega}_C$	=	angular velocity vector of C as seen in A, rad/s

I. Introduction

SPACECRAFT missions such as asteroid surveys, high-inclination solar orbits, and comet rendezvous place enormous demands on conventional chemical propulsion systems. Solar sails have been proposed [1,2] for interplanetary propulsion missions requiring large delta-V and for exotic long-duration non-Keplerian orbits. These missions typically demand very slow thrust-vector reorientation maneuvers, even with time-optimal trajectory planning [3], and have only solar environmental attitude-disturbance torques (due to sail shape aberrations). Slow reorientations enable the sail to be regarded as inertially pointed, as far as attitude dynamics and control are concerned, and a variety of both nonspinning and spinning attitude control methods have been proposed for these missions [4–8].

Although it is an important part of many missions, solar sail operation near planetary bodies is less studied, and this produces additional attitude control disturbances due to the gravity gradient and atmospheric drag. For example, maximum solar torque magnitude on a particular microsailcraft in Earth orbit (see Sec. V) is essentially constant with orbit altitude, at about 10^{-5} Nm. Gravity-gradient torque is inversely proportional to orbit radius cubed, but has maximum magnitude on the order of solar torque in low orbits, becoming relatively insignificant (less than 1%) only above an altitude of about 20,000 km altitude. Aerodynamic torques are exponentially decaying with increasing altitude, dominating (greater than 10 times) both solar and gravity-gradient magnitudes below 500 km, equaling them at about 700 km, and becoming relatively insignificant (less than 1%) above 2000 km.

Uses for solar sails in such proximity to a planet include mission segments such as escape and capture/deorbit. Primary mission modes include long-term orbit maintenance (e.g., to maintain sun

Received 1 December 2007; revision received 3 January 2009; accepted for publication 6 January 2009.

*Associate Professor, Aerospace Engineering Sciences; dale.lawrence@colorado.edu. Associate Fellow AIAA.

†Director, Systems Development and Operational Support; mark.whorton@tbe.com. Associate Fellow AIAA.

synchronicity or to counter the effects of drag) as well as major orbit variations [9]. Indeed, Earth escape was the subject of the earliest technical work in solar sailing [10–12]. And the first experiments, Cosmos I[‡] and Nanosail-D [13],[§] absent launch vehicle failure, were intended to investigate orbit-raising and deorbit capabilities, respectively. In addition, the high cost of large-scale science missions (typically in the range of millions of dollars per kilogram of instrument payload) provides a significant incentive to investigate the potential for small (and mini-, micro-, or nano-) satellite missions that operate, initiate, or terminate in low orbits. Considerable advances have been made in structures, avionics, power, and communication systems, but full realization of the potential cost advantages of small satellites will require fundamental advances in propulsion systems. Miniature sailcraft provide a tantalizing opportunity.

Attitude control of solar sails is challenging in the planetary-disturbance environment. Sailcraft are designed to maximize area-to-mass ratio for the highest lightness factor [1] (or acceleration), resulting in greatly magnified forces due to solar radiation pressure (desired) and aerodynamic drag (undesired). Resulting environmental torques are therefore very sensitive to the c.p.–c.m. offset, which is difficult to predict due to uncertainties in the gossamer-structure deployed shape [14] and shape changes due to solar and aerodynamic pressure-loading [4,8,15,16]. Although solar and aerodynamic torques are usually considered in attitude control, these have been among the smallest disturbances in conventional spacecraft and typically do not drive the design of either the control actuators or the algorithms. The large sailcraft area also tends to push mass properties toward that of a flat plate, resulting in significant gravity-gradient torques.

If the sail is to be inertially pointed throughout the orbit, high-rate spin stabilization can reduce attitude deviations due to orbit-periodic disturbance components. However, spin can only reduce the secular precession *rate* due to constant disturbance components, and control torques must cancel them to maintain long-term inertial pointing. More often, the sail must be repointed periodically during the orbit, making high-rate spin stabilization counterproductive. It would seem, then, that control torques must be sufficiently large to dominate the environmental disturbances and must be correspondingly long-lasting. Periodic components could be provided by reaction wheels, but the long periods imply a large momentum-storage capacity and correspondingly large wheels. Constant components could be provided by reaction jets, with an attendant fuel mass penalty and limit on mission life. Long-duration control torque could be provided by magnetic moments, provided that the planet has a significant magnetic field, or by modulating solar or aerodynamic torque, via changes to the sailcraft c.m.–c.p. offset. Unfortunately, these persistent control torques are limited in direction and are often relatively small in magnitude.

Instead of opposing environmental disturbance torques, this paper describes an approach that *employs* them to produce desirable sail pointing motions. This greatly reduces the requirements on control torque and may provide lower cost and lower mass penalty for operating solar sails in planetary proximity. This approach may also enable unprecedented size and cost reductions in solar sailcraft, catering to the demands of low-cost spacecraft applications that initiate or terminate in low Earth orbit. The idea is to operate the sail in the neighborhood of natural pointing equilibria in the local-vertical/local-horizontal (LVLH) orbiting frame: points at which no control torque is required. Control torque is then only necessary to asymptotically stabilize such equilibria and is only persistent against errors in modeling the environmental torques. Such equilibria were first identified for the gravity-gradient case (no solar or aerodynamic torques) and are called Thompson [17] and Likins–Pringle equilibria [18,19]. These equilibria require the spacecraft to be spinning slowly at certain rates, with the spin-axis aligned with the orbit normal in the Thompson case and with the spin-axis precessing (i.e., coning) at orbit rates in the Likins–Pringle case.

We extend this equilibrium analysis to include both solar and aerodynamic torques, describing the compete set of equilibria in LVLH as a function of spin rate, sailcraft parameters, and orbit characteristics. We also characterize their Lyapunov stability and propose control laws to asymptotically stabilize any of these equilibria. Related work has primarily considered only the gravity-gradient torque equilibria and their stability, for which there is extensive literature going back to 1957 [20,21], concerning rigid and flexible spinners, gyrostats, and nutation damping methods. More limited [22] are investigations combining aerodynamic and gravity-gradient [23,24] or solar and gravity-gradient torques [25,26]. A hybrid aerodynamic-solar stabilization method for elliptic orbits has appeared [27], with aerodynamic torques used near perigee and solar torques used near apogee.

Despite the classical nature of this area, no comprehensive study of the simultaneous action of all three environmental sources on purposeful coning motion has appeared, owing to the unique (and only recently studied) properties and applications of solar sails. Indeed, solar sail coning to influence orbit parameters may constitute the first operational use of Likins–Pringle-type equilibria, for which the practicality for conventional spacecraft has been questioned [21]. Side benefits of spinning operation may include reducing lightness factor (using centripetal tensioning instead of structural mass) and averaging the effects of sail shape aberrations.

When used with a solar sail that is spun about the normal to the sail surface, inertial coning of the sail normal at orbit rates produces useful effects on orbit parameters. Consider the case of an orbit plane nominally perpendicular to the sun vector [12]. Fixing the sail normal in LVLH with a component in the negative orbit velocity direction produces a solar thrust component in the positive velocity direction, increasing orbit energy continuously over time. In the microsailcraft example in Earth orbit, a perfect 40 m^2 sail at 1 AU from the sun produces a maximum solar radiation thrust of approximately 3.6×10^{-4} N. With a 3 kg microsailcraft, this produces an acceleration of 0.12 mm/s^2. Accounting for the component of this acceleration along the orbit velocity, the maximum solar delta-V is about 0.3 m/s per orbit at a 1000 km altitude, resulting in an increase in the semimajor axis of about 0.6 km per orbit, or about 8 km per day. Conversely, if the sail normal has a component along the orbit velocity direction, solar thrust has a component opposing orbital velocity, and the sailcraft orbit spirals inward, providing a positive deorbit capability.

Orienting the sail normal in the radial or antiradial directions produces an effective change in the gravitational constant, enabling formation flight among spacecraft at different orbit radii. Orbit-inclination changes and/or nodal precession occur when the component of the thrust force oriented perpendicular to the orbit plane changes during the orbit, causing an orbit-average precession of the orbit momentum vector. Likewise, eccentricity changes occur when the component of thrust in the plane of the orbit changes during the orbit. These effects can be obtained by half-orbit switching between the LVLH equilibria described here, similar to the original orbit-raising approach [10] and others [9] for low-inclination orbits. Alternatively, a smoother operation would be to cone the sail normal using natural periodic motion at other than orbit rate [26], similar to the orbit-raising approach of [11,28]. Orbit precession is beyond the present scope; only orbit momentum-magnitude changes via orbit-rate coning are considered in this paper.

For interplanetary trajectories, coning of the sail normal can be used to modulate solar thrust magnitude with zero torque [29], in contrast to dithering or orbiting [30] to shed excess thrust, providing increased trajectory controllability [31].

Section II describes key reference frames and attitude dynamics, based on the relevant assumptions on orbit and sailcraft parameters. Section III combines environmental torques with spin-axis precession dynamics to describe the complete set of attitude equilibria in LVLH, identifying operational modes in which the sailcraft can be operated with zero control torque. Rigorous conditions for Lyapunov stability of these equilibria are provided in

[‡]Data available online at http://www.planetary.org/programs/projects/innovative_technologies/solar_sailing/ [retrieved 29 February 2009].

[§]Data available online at http://www.nasa.gov/mission_pages/smallsats/nanosaild.html [retrieved 14 December 2008].

Sec. IV. We show explicitly how equilibrium stability depends on sailcraft and orbit parameters, enabling feasibility analyses and sailcraft/mission design studies. Section V considers the addition of damping control that makes these conditions necessary and ensures asymptotic stability. A complete picture of equilibrium existence and stability as a function of sailcraft spin rate is then given in the form of a bifurcation diagram. We show explicitly how equilibria can be created and destroyed by simply modulating spin rate and how classifying all equilibria and their stability enables a global behavior characterization. The addition of a control potential and associated orientation-dependent control torque is then considered, providing the ability to asymptotically stabilize any of the original equilibria. Robustness of this approach to nonideality is also examined via simulation.

II. Sailcraft Dynamics

A. Reference Frames

Several different reference frames will be used to develop the sailcraft dynamics. Frame A is an Earth-centered inertial frame with $\hat{x}$ and $\hat{y}$ in the equatorial plane, $\hat{z}$ normal to the equatorial plane, and $\hat{x}$ along the vernal equinox. Frame L is the LVLH frame, with $\hat{r}$ in the orbit radial direction, $\hat{v}$ along the sailcraft velocity vector, and $\hat{o}$ aligned with the orbit angular momentum. Frame C is fixed in the sailcraft body, with $\hat{n}$ normal to the plane of the sail and $\hat{p}$ and $\hat{q}$ lying in the plane of the sail. Frame B differs from C only in rotation about $\hat{n}$, to be described subsequently. Figure 1 illustrates these frames.

B. Equations of Motion

For the purposes of this paper, the sailcraft will be assumed to be a rigid body with a uniform, flat, square sail and a sailcraft center of mass located a distance r_c along $\hat{n}$, due to portions of the spacecraft bus located out of the sail plane. The c.p.–c.m. offset r_c scales the aerodynamic and solar environmental torques; its importance as a design parameter is discussed later. As a result of this geometry, the sailcraft moment-of-inertia tensor $\mathbf{I}_s$ has principal axes $\hat{p}$, $\hat{q}$, and $\hat{n}$, and due to the symmetry about $\hat{n}$, frame B is also a principal frame. We define I_n as the principal moment of inertia about $\hat{n}$, and we define I_T as the principal moment of inertia about any transverse principal axis. Typically, the bus is located near the plane of the sail, making the overall inertia tensor similar to that of a flat plate [32], and so $I_n \approx 2I_T$.

Although a sailcraft will be nonrigid by conventional spacecraft standards, the orbit element control application using coning motions produces very smooth low-frequency environmental torques, on the order of orbit frequency, and only requires closed-loop settling times on the order of several orbits. In contrast, attitude stability of a flexible solar sail with much faster settling times can be problematic [33]. Here, the disturbance frequencies and control system bandwidths are on the order of 10^{-4} Hz, and sail lowest structural modes are likely [16,34] to be in the range of 10^{-1} to 10^{-2} Hz for full-size vehicles, and even higher for smaller variants, justifying the rigid-body treatment from a control–structure-interaction viewpoint. Quasi-static effects of sail deformation due to pressure-loading are also important in attitude dynamics, because they cause the center of pressure and center of mass of the sailcraft to vary with attitude [15,16]. As these are secondary effects on sailcraft torque as a function of attitude, the analysis here focuses on the ideal (flat) case. Robustness to these perturbations is considered via simulation studies.

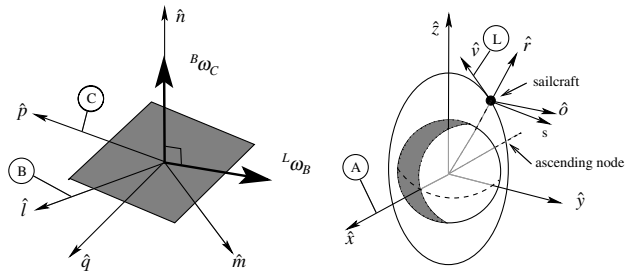

Fig. 1 Reference frames used to develop sailcraft dynamics and performance simulations.

With the inertial angular momentum vector of the body (frame C) as ${}^A\mathbf{h}_C$, the inertial angular velocity vector of the body as ${}^A\boldsymbol{\omega}_C$, net external torques $\boldsymbol{\tau}$, and ${}^A\mathbf{h}_C = \mathbf{I}_s \cdot {}^A\boldsymbol{\omega}_C$, we have the sailcraft dynamics

$$\begin{aligned}\frac{{}^A\mathrm{d}}{\mathrm{d}t}{}^A\mathbf{h}_C = \boldsymbol{\tau} &= \frac{{}^C\mathrm{d}}{\mathrm{d}t}{}^A\mathbf{h}_C + {}^A\boldsymbol{\omega}_C \times {}^A\mathbf{h}_C \\ &= \mathbf{I}_s \cdot \frac{{}^C\mathrm{d}}{\mathrm{d}t}{}^A\boldsymbol{\omega}_C + {}^A\boldsymbol{\omega}_C \times (\mathbf{I}_s \cdot {}^A\boldsymbol{\omega}_C)\end{aligned} \tag{1}$$

hence,

$$\boldsymbol{\tau} = \mathbf{I}_s \cdot \frac{{}^B\mathrm{d}}{\mathrm{d}t}{}^A\boldsymbol{\omega}_C + {}^A\boldsymbol{\omega}_B \times (\mathbf{I}_s \cdot {}^A\boldsymbol{\omega}_C) \tag{2}$$

because $\mathbf{I}_s$ is fixed in C and B. We define frame B such that the relative velocity ${}^L\boldsymbol{\omega}_B$ of B as seen in L is zero along $\hat{n}$, and so B describes the tip and tilt of the sailcraft normal $\hat{n}$ with respect to the LVLH frame L. Additional sailcraft spin about $\hat{n}$ relative to L is purposefully not included in B, because this does not affect the force vector produced by the sail, due to sail symmetry about $\hat{n}$. With ${}^A\boldsymbol{\omega}_L$ given by the orbit rate $\omega_o\hat{o}$, we have the inertial spin about $\hat{n}$ given by

$$\omega_n = \hat{n} \cdot {}^A\boldsymbol{\omega}_C = \hat{n} \cdot ({}^A\boldsymbol{\omega}_L + {}^L\boldsymbol{\omega}_B + {}^B\boldsymbol{\omega}_C) \tag{3}$$

Also define

$$\omega_s = \hat{n} \cdot {}^B\boldsymbol{\omega}_C \tag{4}$$

and

$$\omega_\perp = \hat{n} \cdot {}^A\boldsymbol{\omega}_L = \omega_o\hat{o} \cdot \hat{n} \tag{5}$$

Then

$$\omega_n = \omega_\perp + \omega_s \tag{6}$$

Frames B and C differ only in a rotation about $\hat{n}$. Without loss of generality, we take B to be aligned with C at the initial time epoch t_0.

Taking advantage of the symmetric mass properties, partition

$${}^A\boldsymbol{\omega}_B = \boldsymbol{\omega}_T + \omega_\perp\hat{n}$$

where $\boldsymbol{\omega}_T = (\mathbf{I} - \hat{n}\,\hat{n}) \cdot {}^A\boldsymbol{\omega}_B$. ($\mathbf{I}$ is the identity tensor, and $\hat{n}\,\hat{n}$ is dyadic notation [32], used for a coordinate-free development.) Then

$$\mathbf{I}_s \cdot {}^A\boldsymbol{\omega}_C = I_T\boldsymbol{\omega}_T + I_n\omega_n\hat{n} \tag{7}$$

and

$$\begin{aligned}{}^A\boldsymbol{\omega}_B \times (\mathbf{I}_s \cdot {}^A\boldsymbol{\omega}_C) &= (\boldsymbol{\omega}_T + \omega_\perp\hat{n}) \times (I_T\boldsymbol{\omega}_T + I_n\omega_n\hat{n}) \\ &= (\omega_n I_n - \omega_\perp I_T)\boldsymbol{\omega}_T \times \hat{n}\end{aligned} \tag{8}$$

This results in the dynamics in terms of transverse (orthogonal to $\hat{n}$) and normal (along $\hat{n}$) components:

$$\boldsymbol{\tau}_T = I_T\frac{{}^B\mathrm{d}}{\mathrm{d}t}\boldsymbol{\omega}_T + (\omega_n I_n - \omega_\perp I_T)\boldsymbol{\omega}_T \times \hat{n} \tag{9}$$

$$\tau_n = I_n\dot{\omega}_n \tag{10}$$

III. Precession Equilibria

Ideally, the sail normal $\hat{n}$ is fixed in the L frame, producing inertial coning of $\hat{n}$ at orbit rates. To see if this can be produced by the natural aerodynamic, solar pressure, and gravity-gradient torques, we seek a balance between these orientation-dependent torques and the precession of the sailcraft angular momentum. This is in contrast to the approach in [7], in which constant control torque is necessary to

oppose solar pressure torques in an orbit-raising orientation in LVLH.

Suppose $\hat{n}$ is fixed in L, then B is also fixed in L by definition of the B frame (${}^{L}\boldsymbol{\omega}_{B} \cdot \hat{n} = 0$). Then ${}^{L}\boldsymbol{\omega}_{B} = 0$. Conversely, if ${}^{L}\boldsymbol{\omega}_{B} = 0$, then B is fixed in L, and $\hat{n}$ is fixed in L. When this holds, ${}^{A}\boldsymbol{\omega}_{B} = {}^{A}\boldsymbol{\omega}_{L}$, and so

$$\frac{{}^{B}\mathrm{d}}{\mathrm{d}t}{}^{A}\boldsymbol{\omega}_{B} = \frac{{}^{L}\mathrm{d}}{\mathrm{d}t}{}^{A}\boldsymbol{\omega}_{L} = \frac{{}^{A}\mathrm{d}}{\mathrm{d}t}\omega_o\hat{o} = 0 \tag{11}$$

because $\hat{o}$ is fixed in L and ω_o is constant (a reasonable assumption, because sail forces slowly change the semimajor axis, and hence the orbit period, compared with the orbit rate and the sail attitude motions). Then ${}^{A}\boldsymbol{\omega}_{C} = {}^{A}\boldsymbol{\omega}_{L} + \omega_s\hat{n}$. From Eq. (10), if torque along $\hat{n}$ is zero, then $\omega_n = \omega_s + \omega_\perp$ is constant (hence, ω_s is constant), and

$$\frac{{}^{B}\mathrm{d}}{\mathrm{d}t}{}^{A}\boldsymbol{\omega}_{C} = \frac{{}^{L}\mathrm{d}}{\mathrm{d}t}\omega_s\hat{n} = 0 \tag{12}$$

Using this in Eq. (2), Eq. (9) becomes

$$\boldsymbol{\tau}_T = (\omega_n I_n - \omega_\perp I_T)\boldsymbol{\omega}_T \times \hat{n} \tag{13}$$

Because the aerodynamic and gravity-gradient torques are most naturally specified in L coordinates (see Sec. III.A), we develop the right-hand side of Eq. (13) in these coordinates as follows. Describe $\hat{n}$ in the L frame in terms of a cone angle β and a clock angle ϕ, as shown in Fig. 2. We have the description

$$\hat{n} = -(\sin\beta\sin\phi)\hat{r} + (\sin\beta\cos\phi)\hat{v} + (\cos\beta)\hat{o} \tag{14}$$

Because ${}^{L}\boldsymbol{\omega}_{B} = 0$,

$$\boldsymbol{\omega}_T = (\mathbf{I} - \hat{n}\,\hat{n}) \cdot \omega_o\hat{o} = \omega_o(\hat{o} - \cos\beta\hat{n})$$

$$\boldsymbol{\omega}_T \times \hat{n} = -\omega_o \sin\beta(\cos\phi\hat{r} + \sin\phi\hat{v})$$

and

$$\omega_\perp = \omega_o\hat{o} \cdot \hat{n} = \omega_o\cos\beta$$

Thus, for $\hat{n}$ and ω_s to remain fixed in L, normal torques must be zero and transverse torques must satisfy

$$\boldsymbol{\tau}_T = -(\omega_s I_n + \omega_o\cos\beta(I_n - I_T))\omega_o\sin\beta(\cos\phi\hat{r} + \sin\phi\hat{v}) \tag{15}$$

Using Eq. (6), this becomes

$$\boldsymbol{\tau}_T = -(\omega_n I_n - \omega_o I_T\cos\beta)\omega_o\sin\beta(\cos\phi\hat{r} + \sin\phi\hat{v}) \tag{16}$$

A. Environmental Torques

The aerodynamic torques $\boldsymbol{\tau}_a$ on the sailcraft depend [21,35] on the orientation of the sail normal $\hat{n}$ relative to the aerodynamic force vector, which is approximately directed along the sailcraft velocity vector $\hat{v}$, resulting in

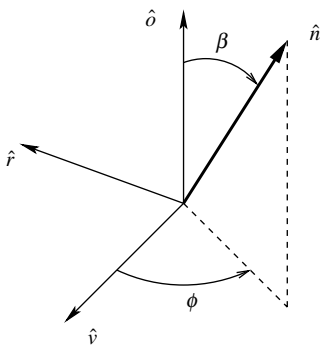

Fig. 2 Cone and clock angles of the sail normal $\hat{n}$ relative to the LVLH frame L.

$$\boldsymbol{\tau}_a = -\tau_{\mathrm{am}}|\hat{v}\cdot\hat{n}|\hat{v}\times\hat{n} \tag{17}$$

where $\tau_{\mathrm{am}} = 1/2 r_c\rho C_D v^2 A_s \geq 0$ is the aerodynamic moment coefficient. Using Eq. (14) and noting that $\beta \in [0, \pi]$ (forces can impinge on either the front or the back of the sail), we obtain

$$\boldsymbol{\tau}_a = -\tau_{\mathrm{am}}\sin\beta|\cos\phi|(\cos\beta\hat{r} + \sin\beta\sin\phi\hat{o}) \tag{18}$$

Similarly, solar torque $\boldsymbol{\tau}_s$ depends [21,35] on the orientation of $\hat{n}$ relative to the sailcraft-to-sun vector $\hat{s}$:

$$\boldsymbol{\tau}_s = -\tau_{\mathrm{sm}}|\hat{s}\cdot\hat{n}|\hat{s}\times\hat{n} \tag{19}$$

where $\tau_{\mathrm{sm}} = r_c(1 - f_s)PA_s \geq 0$ is the solar moment coefficient. More complex models can be used [2,14] for the optical properties, although the simple model captures the principal effects. Higher-order variations can be considered as perturbations. Assuming that the orbit is normal to the sun (i.e., $\hat{s} = \hat{o}$), we have

$$\boldsymbol{\tau}_s = \tau_{\mathrm{sm}}\sin\beta|\cos\beta|(\cos\phi\hat{r} + \sin\phi\hat{v}) \tag{20}$$

Orbit–sun vector misalignment can be a significant effect and is treated as a perturbation in Sec. V.D.

Gravity-gradient torques $\boldsymbol{\tau}_g$ are given by [21,35]

$$\boldsymbol{\tau}_g = \frac{3\mu}{a^3}[\hat{r}\times(\mathbf{I}_s\cdot\hat{r})] \tag{21}$$

Write

$$\mathbf{I}_s = I_n\hat{n}\,\hat{n} + I_T(\mathbf{I} - \hat{n}\,\hat{n}) = (I_n - I_T)\hat{n}\,\hat{n} + I_T\mathbf{I} \tag{22}$$

and use $\omega_o = \sqrt{\mu/a^3}$ to obtain

$$\boldsymbol{\tau}_g = 3\omega_o^2(I_n - I_T)(\hat{r}\cdot\hat{n})\hat{r}\times\hat{n} \tag{23}$$

This results in

$$\boldsymbol{\tau}_g = 3\tau_{\mathrm{gm}}\sin\beta\sin\phi(\cos\beta\hat{v} - \sin\beta\cos\phi\hat{o}) \tag{24}$$

where the gravity-gradient moment coefficient

$$\tau_{\mathrm{gm}} = \omega_o^2(I_n - I_T) \geq 0$$

depends on sailcraft mass properties and orbit radius.

B. Equilibrium Spin

For the net torque $\boldsymbol{\tau} = \boldsymbol{\tau}_a + \boldsymbol{\tau}_s + \boldsymbol{\tau}_g$ to satisfy Eq. (16), we have three simultaneous equations from the three vector components, and the inertial spin ω_n can be freely chosen. The solution for equilibrium spin ω_{no} must satisfy the following:

For the $\hat{r}$ component,

$$-(\omega_{no}I_n - \omega_o I_T\cos\beta)\omega_o\sin\beta\cos\phi = -\tau_{\mathrm{am}}\sin\beta\cos\beta|\cos\phi| + \tau_{\mathrm{sm}}\sin\beta|\cos\beta|\cos\phi \tag{25}$$

For the $\hat{v}$ component,

$$-(\omega_{no}I_n - \omega_o I_T\cos\beta)\omega_o\sin\beta\sin\phi = \tau_{\mathrm{sm}}\sin\beta|\cos\beta|\sin\phi + 3\tau_{\mathrm{gm}}\sin\beta\cos\beta\sin\phi \tag{26}$$

For the $\hat{o}$ component,

$$0 = -\tau_{\mathrm{am}}\sin^2\beta|\cos\phi|\sin\phi - 3\tau_{\mathrm{gm}}\sin^2\beta\cos\phi\sin\phi \tag{27}$$

A given cone β and clock ϕ angle orientation of $\hat{n}$ in L is an equilibrium solution to the attitude dynamics if a spin rate ω_{no} exists to satisfy the preceding three equations for arbitrary values of τ_{am}, τ_{sm}, I_n, I_T, and ω_o. Cases in which equilibrium occurs due to particular relationships between these parameters are excluded, because this would require specific orbit and sailcraft properties that would be unlikely to occur in practice. Equilibria are classified as follows.

For type I with $\sin\beta = 0$, $\hat{n}$ is inertially pointed, and hence there is no coning. This corresponds to conventional spin stabilization, with inertial spin rate ω_{no}. All three constraints are satisfied for any ϕ and any ω_{no}. Type I.A with $\beta = 0$ has orbit normal pointing. Type I.B with $\beta = \pi$ has antiorbit normal pointing.

For type II with $\cos\beta = 0$, $\hat{n}$ lies in the plane of the orbit, and the sail is edge-on to the sun (no solar thrust), rotating in the inertial frame about an axis in the plane of the sail at orbit rate. This requires $\omega_{no} = 0$ and $\cos\phi\sin\phi = 0$. Type II.A with $\sin\phi = 0$ has velocity or antivelocity pointing. This provides maximum aerodynamic drag that can be used to ensure that the sailcraft deorbits in a reasonable time, mitigating orbital debris concerns. Type II.B with $\cos\phi = 0$ has nadir or antinadir pointing. This may be useful for viewing the deployed sail from ground telescopes or for ground observation by onboard instruments.

Type III with $\cos\beta\sin\beta \neq 0$ requires $\cos\phi\sin\phi = 0$. The sail normal cones in the inertial frame at orbit rate, and solar thrust is produced. For type III.A, $\sin\phi = 0$. Type III.A.1 with $\phi = 0$ produces a component of the solar thrust vector in the antivelocity direction, reducing orbit energy, hence reducing the orbit semimajor axis a. This requires the equilibrium spin rate

$$\omega_{no} = \frac{\cos\beta}{I_n\omega_o}(\omega_o^2 I_T + \tau_{\text{am}} - \tau_{\text{sm}}\text{sign}(\cos\beta)) \tag{28}$$

Type III.A.2 with $\phi = \pi$ produces a component of solar thrust in the velocity direction, increasing orbit energy and a over time. This requires a spin rate

$$\omega_{no} = \frac{\cos\beta}{I_n\omega_o}(\omega_o^2 I_T - \tau_{\text{am}} - \tau_{\text{sm}}\text{sign}(\cos\beta)) \tag{29}$$

Type III.B with $\cos\phi = 0$ produces a component of solar thrust in the radial or antiradial directions. The required spin rate is

$$\omega_{no} = \frac{\cos\beta}{I_n\omega_o}(\omega_o^2 I_T - 3\tau_{\text{gm}} - \tau_{\text{sm}}\text{sign}(\cos\beta)) \tag{30}$$

The complete set of equilibria is shown in Fig. 3.

Any particular equilibrium shown in Fig. 3 can be obtained by suitable selection of the spin rate ω_{no}. Conversely, selection of the spin rate ω_{no} produces particular (usually, several) equilibria, with corresponding values of β and ϕ. Although behavior in the neighborhood of a desired equilibrium is characterized by the stability properties of that equilibrium (discussed in Sec. IV), global behavior will depend on the existence and stability of any other (potentially undesired) equilibria.

From the preceding conditions, two type I equilibria exist for all ω_{no}, type II exist only for $\omega_{no} = 0$, and type III exist only for ω_{no} in the intervals between zero and

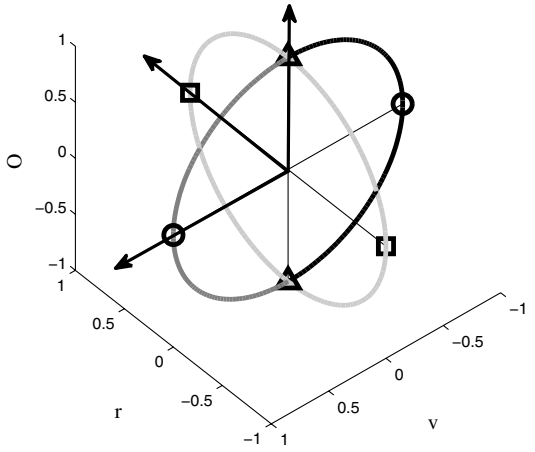

Fig. 3 Equilibria of the sail normal $\hat{n}$ in the LVLH frame L: type I (triangles), type II.A (small circles), type II.B (squares), type III.A.1 (medium gray line), type III.A.2 (black line), and type III.B (light gray line).

$$\frac{\omega_o^2 I_T + \tau_{\text{am}} - \tau_{\text{sm}}}{\omega_o I_n} \tag{31a}$$

for type III.A.1 with $\cos\beta > 0$.

$$\frac{-\omega_o^2 I_T - \tau_{\text{am}} - \tau_{\text{sm}}}{\omega_o I_n} \tag{31b}$$

for type III.A.1 with $\cos\beta < 0$.

$$\frac{\omega_o^2 I_T - \tau_{\text{am}} - \tau_{\text{sm}}}{\omega_o I_n} \tag{31c}$$

for type III.A.2 with $\cos\beta > 0$.

$$\frac{-\omega_o^2 I_T + \tau_{\text{am}} - \tau_{\text{sm}}}{\omega_o I_n} \tag{31d}$$

for type III.A.2 with $\cos\beta < 0$.

$$\frac{\omega_o^2 I_T - 3\tau_{\text{gm}} - \tau_{\text{sm}}}{\omega_o I_n} \tag{31e}$$

for type III.B with $\cos\beta > 0$.

$$\frac{-\omega_o^2 I_T + 3\tau_{\text{gm}} - \tau_{\text{sm}}}{\omega_o I_n} \tag{31f}$$

for type III.B with $\cos\beta < 0$.

Thus, if a type I equilibrium is desired, ω_{no} can be chosen to be sufficiently large (or small) so that no other types of equilibria exist.

As ω_{no} decreases from large values, other equilibria bifurcate into existence. Note that at least one of the intervals in each pair is negative, due to the $-\tau_{\text{sm}}$ offset. If any of the upper boundaries of the intervals (31) are positive, as ω_{no} enters the upper boundary, equilibria are born at $|\cos\beta| = 1$ and move toward $\cos\beta = 0$, and the equilibrium becomes type II as ω_{no} becomes zero. As ω_{no} becomes negative, type II equilibria become type III again and move toward $|\cos\beta| = 1$ with the opposite sign. The equilibrium ceases to exist as ω_{no} crosses the lower threshold of the interval of existence. For interval pairs with zero upper boundaries, equilibria bifurcate into existence in pairs at $\cos\beta = 0$ as ω_{no} crosses zero, and both move toward $|\cos\beta| = 1$ with opposite signs, ceasing to exist as ω_{no} crosses the lower threshold of the respective interval of existence.

A maximum of 10 equilibria may exist for any particular value of ω_{no} (two for type I; two each for type III.A.1, type III.A.2, and type III.B with $\phi = \pi/2$; and type III.B with $\phi = -\pi/2$). Six exist when $\omega_{no} = 0$ (two for type I, and two each for types II.A and II.B).

Orbit and sailcraft design choices affect the parameters τ_{am}, τ_{sm}, and τ_{gm}, influencing the set of feasible equilibria. The c.p.–c.m. offset on the sailcraft scales τ_{am} and τ_{sm} relative to τ_{gm}. The case of a zero c.p.–c.m. offset was treated in [29], in which gravity-gradient torque $3\tau_g$ was also assumed to be zero (approximated by a sailcraft in a solar orbit in which ω_o is very small). This produces $\tau_{\text{am}} = \tau_{\text{sm}} = 0$, and the $3\tau_{\text{gm}}$ gravity-gradient term disappears from Eq. (30), leaving the two type I equilibria and (possibly, depending on ω_{no}) a single remaining equilibrium satisfying

$$\omega_{no} = \frac{\cos\beta}{I_n\omega_o}\omega_o^2 I_T = \omega_o\cos\beta\frac{I_T}{I_n} \tag{32}$$

where ω_o in this case is the desired coning rate of the sail normal, not the orbit rate.

For circular planetary orbits, with a zero c.p.–c.m. offset, the gravity-gradient torque $3\tau_{\text{gm}}$ reappears in Eq. (30), but τ_{am} and τ_{sm} remain zero in Eqs. (28–30). The type I equilibria in this case were first analyzed by Thompson [17]. Types III.A.1 and A.2 equilibria have the same conditions as Eq. (32), but type III.B equilibria are distinguished by a different ω_{no}. These equilibria are also well known in this case and are referred to as Likins–Pringle equilibria [18,19], with type III.A denoted as hyperbolic, because the spin-axis appears to trace a hyperboloid in inertial space as the spin axis moves

with the spacecraft along the orbit. Similarly, type III.B has been denoted as conical, due to the set described by the spin axis in A along the orbit. Both are described here as coning in A, because the spin axis traces a cone in A when A remains centered at the sailcraft center of mass.

When the c.p.–c.m. offset is nonzero, but the orbit is high relative to the planet's atmosphere, $\tau_{\rm sm}$ becomes nonzero in type III equilibrium conditions. This produces additional equilibria, owing to the $|\cos\beta|$ dependence in the solar torque. If the c.p.–c.m. offset and sail area are small enough, $\tau_{\rm sm} < \omega_o^2 I_T$ and type III.A equilibria exist with both prograde and retrograde inertial spin ω_{no} with respect to ω_o. Otherwise, ω_{no} is nonpositive (retrograde). Similarly, ω_{no} has both signs for type III.B equilibria when $\tau_{\rm sm} < \omega_o^2 I_T - 3\tau_{\rm gm}$, and ω_{no} is nonpositive otherwise.

For lower orbits, atmospheric torques become significant, and the $\tau_{\rm am}$ terms in type III.A equilibrium conditions enlarge the intervals of existence. Type III.B equilibrium existence is unaffected.

IV. Stability of Equilibria

Stability of an equilibrium can be determined by studying linearized dynamics, provided that the equilibrium is hyperbolic [36]. Because of the absence of damping, many of the equilibria in this system have center manifolds (neutrally stable linearizations); hence, the linearized stability analysis is inconclusive. Also, analytic stability conditions are complicated by eigenvalue determination. Instead, we take a direct Lyapunov approach, which provides sufficient analytic conditions for stability. Our strategy for finding a suitable Lyapunov function is motivated by Hughes [21], although we use a coordinate-free approach that provides a more transparent development. Also, the B frame used here is similar, but not the same as the stroboscopic frame S used there. More significantly, we include the effects of aerodynamic and solar environmental torques on stability, in addition to the gravity-gradient potential.

A Lyapunov function candidate is constructed in two parts, corresponding to the kinetic energy of the spacecraft relative to a desired equilibrium condition and to the potential energy from the aerodynamic, solar, and gravity-gradient torques:

$$V_1 = \tfrac{1}{2}{}^L\boldsymbol{\omega}_B \cdot \mathbf{I}_s \cdot {}^L\boldsymbol{\omega}_B \tag{33}$$

$$V_2 = \Psi_a + \Psi_s + \Psi_g + \Psi_x + \tfrac{1}{2}I_n(\omega_s - \omega_{so})^2 - \tfrac{1}{2}{}^A\boldsymbol{\omega}_L \cdot \mathbf{I}_s \cdot {}^A\boldsymbol{\omega}_L + V_o \tag{34}$$

Clearly, the kinetic term V_1 is zero when the B frame is fixed in L. The Ψ_a, Ψ_s, and Ψ_g terms are potential functions that describe the aerodynamic, solar, and gravity-gradient torques as functions of the sail normal $\hat{n}$ attitude as follows:

$$\Psi_a = \tfrac{1}{2}\tau_{\rm am}(1 - \text{sign}(\hat{n}\cdot\hat{v})(\hat{n}\cdot\hat{v})^2) \tag{35}$$

$$\Psi_s = \tfrac{1}{2}\tau_{\rm sm}(1 - \text{sign}(\hat{n}\cdot\hat{s})(\hat{n}\cdot\hat{s})^2) \tag{36}$$

$$\Psi_g = \tfrac{3}{2}\omega_o^2((I_n - I_T)(\hat{r}\cdot\hat{n})^2 + I_T) \tag{37}$$

where Ψ_x and the quadratic term in ${}^A\boldsymbol{\omega}_L$ are extra terms needed to account for the noninertial reference for the kinetic energy in V_1, and Ψ_x is chosen to cancel a particular term, as discussed later:

$$\Psi_x = -\omega_o\omega_{so}I_n\hat{o}\cdot\hat{n} \tag{38}$$

Note that the ${}^A\boldsymbol{\omega}_L$ term in Eq. (34) appears to be kinetic, but is actually a potential because ${}^A\boldsymbol{\omega}_L = \omega_o\hat{o}$ is inertially fixed, and so this term depends on the variation in the inertia tensor $\mathbf{I}_s$ as the orientation of $\hat{n}$ varies:

$$-\tfrac{1}{2}{}^A\boldsymbol{\omega}_L \cdot \mathbf{I}_s \cdot {}^A\boldsymbol{\omega}_L = -\tfrac{1}{2}\omega_o^2((I_n - I_T)(\hat{o}\cdot\hat{n})^2 + I_T) \tag{39}$$

Likewise, the $\omega_s - \omega_{so}$ term is actually a potential, because

$$(\omega_s - \omega_{so})^2 = (\hat{o}\cdot(\hat{n}_o - \hat{n}))^2 \tag{40}$$

and $\hat{n}_o$ is the equilibrium orientation corresponding to the spin rate ω_{so}. V_o is a constant that depends on the equilibrium for which the stability is to be analyzed (so that V_2 is zero at the equilibrium of interest).

The external torques (17), (19), and (21) are obtained from Eqs. (35–37), respectively, via

$$\boldsymbol{\tau}_a = \frac{\partial\Psi_a}{\partial\hat{n}} \times \hat{n} \tag{41}$$

$$\boldsymbol{\tau}_s = \frac{\partial\Psi_s}{\partial\hat{n}} \times \hat{n} \tag{42}$$

$$\boldsymbol{\tau}_g = \frac{\partial\Psi_g}{\partial\hat{n}} \times \hat{n} \tag{43}$$

The Lyapunov function candidate is then $V = V_1 + V_2$, and we compute its time derivative as follows. First, we rearrange V into the two terms

$$V_a = \tfrac{1}{2}{}^L\boldsymbol{\omega}_B \cdot \mathbf{I}_s \cdot {}^L\boldsymbol{\omega}_B + \tfrac{1}{2}I_n\omega_s^2 - \tfrac{1}{2}{}^A\boldsymbol{\omega}_L \cdot \mathbf{I}_s \cdot {}^A\boldsymbol{\omega}_L \tag{44}$$

$$V_b = \Psi_a + \Psi_s + \Psi_g + \Psi_x - \omega_s\omega_{so}I_n + \tfrac{1}{2}I_n\omega_{so}^2 + V_o \tag{45}$$

Because ${}^L\boldsymbol{\omega}_C = {}^L\boldsymbol{\omega}_B + \omega_s\hat{n}$, and these two components are always orthogonal by definition of the B frame, we have

$$V_a = \tfrac{1}{2}{}^L\boldsymbol{\omega}_C \cdot \mathbf{I}_s \cdot {}^L\boldsymbol{\omega}_C - \tfrac{1}{2}{}^A\boldsymbol{\omega}_L \cdot \mathbf{I}_s \cdot {}^A\boldsymbol{\omega}_L \tag{46}$$

Because ${}^L\boldsymbol{\omega}_C = {}^A\boldsymbol{\omega}_C - {}^A\boldsymbol{\omega}_L$,

$$V_a = \tfrac{1}{2}{}^A\boldsymbol{\omega}_C \cdot \mathbf{I}_s \cdot {}^A\boldsymbol{\omega}_C - {}^A\boldsymbol{\omega}_C \cdot \mathbf{I}_s \cdot {}^A\boldsymbol{\omega}_L \tag{47}$$

Taking the time derivative of the scalar V_a with respect to the C frame (any frame may be used, because V_a is scalar) and noting that $\mathbf{I}_s$ is fixed in C, we obtain

$$\frac{\mathrm{d}}{\mathrm{d}t}V_a = ({}^A\boldsymbol{\omega}_C - {}^A\boldsymbol{\omega}_L)\cdot\mathbf{I}_s\cdot\frac{{}^C\mathrm{d}}{\mathrm{d}t}{}^A\boldsymbol{\omega}_C - {}^A\boldsymbol{\omega}_C\cdot\mathbf{I}_s\cdot\frac{{}^C\mathrm{d}}{\mathrm{d}t}{}^A\boldsymbol{\omega}_L \tag{48}$$

Using the sailcraft dynamics (1) for the derivative in the first term, and expressing the derivative in the second term relative to the L frame yields

$$\frac{\mathrm{d}}{\mathrm{d}t}V_a = {}^L\boldsymbol{\omega}_C\cdot(\boldsymbol{\tau} - {}^A\boldsymbol{\omega}_C\times(\mathbf{I}_s\cdot{}^A\boldsymbol{\omega}_C)) + {}^A\boldsymbol{\omega}_C\cdot\mathbf{I}_s\cdot({}^L\boldsymbol{\omega}_C\times{}^A\boldsymbol{\omega}_L) \tag{49}$$

With the vector identity $\mathbf{a}\cdot(\mathbf{b}\times\mathbf{c}) = \mathbf{c}\cdot(\mathbf{a}\times\mathbf{b})$ we obtain

$$\frac{\mathrm{d}}{\mathrm{d}t}V_a = {}^L\boldsymbol{\omega}_C\cdot\boldsymbol{\tau} \tag{50}$$

For V_b, substitute $\omega_s = \omega_n - \omega_o\hat{o}\cdot\hat{n}$ in Eq. (45), and use Eq. (38) to cancel the resulting $\omega_{so}\omega_o I_n\hat{o}\cdot\hat{n}$ term. Then

$$\frac{\mathrm{d}}{\mathrm{d}t}V_b = \frac{\partial\Psi_a}{\partial\hat{n}}\cdot\frac{{}^L\mathrm{d}}{\mathrm{d}t}\hat{n} + \frac{\partial\Psi_a}{\partial\hat{v}}\cdot\frac{{}^L\mathrm{d}}{\mathrm{d}t}\hat{v} + \frac{\partial\Psi_s}{\partial\hat{n}}\cdot\frac{{}^L\mathrm{d}}{\mathrm{d}t}\hat{n} + \frac{\partial\Psi_s}{\partial\hat{s}}\cdot\frac{{}^L\mathrm{d}}{\mathrm{d}t}\hat{s} + \frac{\partial\Psi_g}{\partial\hat{n}}\cdot\frac{{}^L\mathrm{d}}{\mathrm{d}t}\hat{n} + \frac{\partial\Psi_g}{\partial\hat{r}}\cdot\frac{{}^L\mathrm{d}}{\mathrm{d}t}\hat{r} - \omega_{so}I_n\frac{\mathrm{d}}{\mathrm{d}t}\omega_n \tag{51}$$

Because $\hat{v}$, $\hat{s}$, and $\hat{r}$ are fixed in L, the second, fourth, and sixth terms in Eq. (51) are zero. Because $\hat{n}$ is fixed in C, writing the L frame derivatives in terms of the C frame derivatives and using the vector identity $\mathbf{a}\cdot(\mathbf{b}\times\mathbf{c}) = -\mathbf{b}\cdot(\mathbf{a}\times\mathbf{c})$ results in

$$\frac{\mathrm{d}}{\mathrm{d}t}V_b = -{}^L\boldsymbol{\omega}_C \cdot \left(\frac{\partial \Psi_a}{\partial \hat{n}} \times \hat{n} + \frac{\partial \Psi_s}{\partial \hat{n}} \times \hat{n} - \frac{\partial \Psi_g}{\partial \hat{r}} \times \hat{r}\right) - \omega_{so} I_n \frac{\mathrm{d}}{\mathrm{d}t}\omega_n \tag{52}$$

Substituting the expressions (41–43) for the constituents of $\boldsymbol{\tau}$ and noting that these torques are always orthogonal to $\hat{n}$, and so ω_n is constant from Eq. (10), we arrive at this rather remarkable result:

$$\frac{\mathrm{d}}{\mathrm{d}t}V = \frac{\mathrm{d}}{\mathrm{d}t}(V_a + V_b) = 0 \tag{53}$$

Hence, V is a constant of the motion under the solar, aerodynamic, and gravity-gradient torques. In retrospect, it is perhaps not surprising that this system should have a Hamiltonian function V that is conserved, because it is a rigid body with conservative aerodynamic, solar, and gravity-gradient fields. The complication of finding an appropriate V arises from the use of a noninertial reference frame L in which to measure relative kinetic energy. This relative formulation works as long as frame L has an angular velocity vector ${}^A\boldsymbol{\omega}_L$ fixed in the inertial frame A.

Given Eq. (53), if V is a positive-definite function of ${}^L\boldsymbol{\omega}_B$ and deviations of $\hat{n}$ from $\hat{n}_o$, in a neighborhood of $\mathbf{0}$ and $\hat{n}_o$, respectively, then the equilibrium in L is Lyapunov stable [37]. Because $\mathbf{I}_s$ is positive definite, Eq. (34) is a positive-definite function of ${}^L\boldsymbol{\omega}_B$, and so the only question is whether the potential function V_2 in Eq. (34) is positive definite in deviations of $\hat{n}$ from $\hat{n}_o$.

Consider the case of equilibrium type I.A characterized by $\beta = 0$ (orbit normal pointing for $\hat{n}$). Let $\hat{n}$ deviate from the equilibrium $\hat{n}_o = \hat{o}$ as follows:

$$\hat{n} = (1 - \epsilon)\hat{o} + \delta_n \tag{54}$$

where the deviation vector δ_n is orthogonal to $\hat{n}_o$, given in this case by $\delta_n = \delta_1 \hat{v} + \delta_2 \hat{r}$. To preserve unity magnitude, $(1-\epsilon)^2 = 1 - \delta_n \cdot \delta_n$. This implies

$$\epsilon = \tfrac{1}{2}(\delta_1^2 + \delta_2^2) + O|\delta_n|^3 \tag{55}$$

The arguments of the potential terms in Eqs. (35–39) are then

$$\hat{n} \cdot \hat{v} = \delta_1 \qquad \hat{n} \cdot \hat{o} = 1 - \epsilon \qquad \hat{n} \cdot \hat{r} = \delta_2$$

Inserting these into V_2 and expanding to second order in the deviation $|\delta_n|$ results in

$$\begin{aligned} V_2 = {} & \frac{1}{2}(\tau_{\mathrm{am}} - \omega_o^2(I_n - I_T) - 2\omega_o\omega_{so}I_n + 2\omega_o^2 I_T) \\ & + \frac{\delta_1^2}{2}(-\tau_{\mathrm{am}}\mathrm{sign}(\delta_1) + \tau_{sm} + \omega_o^2(I_n - I_T) + \omega_o\omega_{so}I_n) \\ & + \frac{\delta_2^2}{2}(\tau_{\mathrm{sm}} + 4\omega_o^2(I_n - I_T) + \omega_o\omega_{so}I_n) + O|\delta_n|^3 \end{aligned} \tag{56}$$

Thus, this equilibrium is Lyapunov stable if the quadratic deviation coefficients are positive. Using Eq. (6), the condition becomes

$$\begin{aligned} -\tau_{\mathrm{am}} + \tau_{\mathrm{sm}} - \omega_o^2 I_T + \omega_{no}\omega_o I_n > 0 \quad \text{and} \\ \tau_{\mathrm{sm}} + 3\omega_o^2 I_n - 4\omega_o^2 I_T + \omega_{no}\omega_o I_n > 0 \end{aligned} \tag{57}$$

The second condition is implied by the first (when $I_n \geq I_T$), so that a large-enough spin ω_{no} stabilizes this equilibrium for any orbit altitude, mass properties, and aerodynamic and solar torques.

A similar argument for type I.B equilibrium leads to the sufficient condition

$$-\tau_{\mathrm{am}} - \tau_{\mathrm{sm}} - \omega_o^2 I_T - \omega_{no}\omega_o I_n > 0 \tag{58}$$

for Lyapunov stability. Here, a sufficiently negative (retrograde) spin ω_{no} ensures stability. A spinning solar sail operating in the neighborhood of a type I equilibrium was considered in [4,8], although no aerodynamic forces were included. The solar torques were also considered to be constant in the body frame, independent of attitude, and so stability of this equilibrium could not be investigated.

For type II equilibria, the same approach is used, except that these require that $\omega_{no} = 0$ at equilibrium. The sufficient conditions for Lyapunov stability are as follows.

Type II.A.1 is the velocity pointing of $\hat{n}_o$:

$$\tau_{\mathrm{am}} - \tau_{\mathrm{sm}} + \omega_o^2 I_T > 0 \quad \text{and} \quad \tau_{\mathrm{am}} + 3\tau_{\mathrm{gm}} > 0 \tag{59}$$

Type II.A.2 is the antivelocity pointing of $\hat{n}_o$:

$$-\tau_{\mathrm{am}} - \tau_{\mathrm{sm}} + \omega_o^2 I_T > 0 \quad \text{and} \quad -\tau_{\mathrm{am}} + 3\tau_{\mathrm{gm}} > 0 \tag{60}$$

Type II.B is the nadir or antinadir pointing of $\hat{n}_o$:

$$-\tau_{\mathrm{sm}} - 3\tau_{\mathrm{gm}} + \omega_o^2 I_T > 0 \quad \text{and} \quad -\tau_{\mathrm{am}} - 3\tau_{\mathrm{gm}} > 0 \tag{61}$$

Note that Eq. (61) cannot be satisfied, and Eqs. (59) and (60) are affected oppositely by aerodynamic drag, but both are destabilized by a sufficiently large solar torque.

The same approach can be taken for type III equilibria, except that to ensure the sign functions in Eqs. (35) and (36) do not change on a neighborhood under consideration, sufficiently small deviations about the equilibrium are required. When the equilibrium conditions are substituted for ω_{so}, terms linear in the deviations cancel, leaving quadratic terms that are positive under the following conditions:

For type III.A.1, where $\phi = 0$,

$$\tau_{\mathrm{am}} - \tau_{\mathrm{sm}}\mathrm{sign}(\cos(\beta)) + \omega_o^2 I_T > 0 \quad \text{and} \quad \tau_{\mathrm{am}} + 3\tau_{\mathrm{gm}} > 0 \tag{62}$$

For type III.A.2, where $\phi = \pi$,

$$-\tau_{\mathrm{am}} - \tau_{\mathrm{sm}}\mathrm{sign}(\cos(\beta)) + \omega_o^2 I_T > 0 \quad \text{and} \quad -\tau_{\mathrm{am}} + 3\tau_{\mathrm{gm}} > 0 \tag{63}$$

For type III.B, where $\cos(\phi) = 0$,

$$-\tau_{\mathrm{sm}} - 3\tau_{\mathrm{gm}} + \omega_o^2 I_T > 0 \quad \text{and} \quad -\tau_{\mathrm{am}} - 3\tau_{\mathrm{gm}} > 0 \tag{64}$$

Note that Eq. (64) cannot be satisfied, and Eqs. (62) and (63) are again oppositely affected by aerodynamic torque. It is interesting to note that the solar torque is destabilizing for equilibria in which $\cos\beta > 0$, but it is stabilizing for $\cos\beta < 0$. Aerodynamic torque is destabilizing, except for type III.A.1 and type II.A.1 equilibria.

Because Eqs. (58–64) are only sufficient conditions for stability, failure does not imply instability. In the next section, control is applied to provide damping, which enables sharper Lyapunov stability results to be obtained, as well as asymptotic stability. The addition of a control potential term is also discussed, which enables any of the equilibria in L to be stabilized.

V. Feedback Control

A. Spin Rate Control

From Eq. (10), spin rate ω_n can be controlled independently by the application of control torque τ_n along $\hat{n}$. On a sailcraft, these torques can be produced by a pinwheel configuration of sail sectors, as in the heliogyro [38] or T-bar [7] concepts. If the spin rate is only rarely changed in the mission, conventional thrusters may suffice.

Given that highly precise pointing is not required for most sailcraft missions (and this would be difficult to accomplish in the presence of sail shape variations) and that the equilibrium orientation is a continuous function of spin rate ω_{no} from Sec. III, a simple proportional spin rate control is suggested:

$$\tau_n = k_s(\omega_{no} - \omega_n) \tag{65}$$

This causes spin rate error $\omega_{no} - \omega_n$ to decay to zero at the exponential rate $e^{-(k_s/I_n)t}$, because Eq. (65) in Eq. (10) produces a linear system with the characteristic polynomial $s + k_s/I_n$.

B. Damping Control

Torques transverse to the sail normal can be produced by conventional thrusters or momentum-exchange devices, although these may be inappropriate for long-term use on solar sails, due to the

mass of expendable fuel or the large momentum capacity required [4,8,29]. Solar and aerodynamic control torques use variation in the c.p.–c.m. offset, requiring no fuel or momentum storage. Concepts for conventional spacecraft have used movable reflective or drag panels [23–25,27], and solar sail concepts have used a portion of sail area dedicated to moveable vanes [4,8,31,39,40]. A complementary approach is to move mass in the sailcraft relative to the sail (e.g., by mounting the sailcraft bus on a gimballed mast [4,8,40] or by translating ballast masses). Our interest here is the fundamental effect of applying damping control torques transverse to the sail normal, and so details of various torque actuation methods are not pursued. Consider the simple proportional damping control law relative to the desired equilibrium in L:

$$\boldsymbol{\tau}_{c1} = -k_d {}^L\boldsymbol{\omega}_B \qquad k_d > 0 \tag{66}$$

When added to the external torques $\boldsymbol{\tau}$ in Eq. (50), this control produces

$$\frac{\mathrm{d}}{\mathrm{d}t} V = -k_d({}^L\boldsymbol{\omega}_B + {}^B\boldsymbol{\omega}_C) \cdot {}^L\boldsymbol{\omega}_B = -k_d {}^L\boldsymbol{\omega}_B \cdot {}^L\boldsymbol{\omega}_B \tag{67}$$

because ${}^B\boldsymbol{\omega}_C$ is orthogonal to ${}^L\boldsymbol{\omega}_B$. We can now use the LaSalle invariance principle to clarify the stability properties of equilibria in L. First, because $\dot{V} \leq 0$ and the potential component V_2 is lower-bounded (due to $\hat{n}$ being confined to the unit sphere $S^2 \subset R^3$), V_1 is upper-bounded beginning at any initial state. Because V_1 is a positive-definite function of ${}^L\boldsymbol{\omega}_B$, these state components are also bounded. Note that because ${}^L\boldsymbol{\omega}_B$ is zero along $\hat{n}$, this angular velocity vector evolves in the plane normal to $\hat{n}$. Thus, there exists a compact set Ω of states

$$({}^L\boldsymbol{\omega}_B, \hat{n}) \in R^2 \times S^2$$

that is positively invariant. By LaSalle (see, for example, [37]), the state converges to the largest invariant set such that $\dot{V} = 0$ in Eq. (67) (i.e., ${}^L\boldsymbol{\omega}_B = 0$). From Sec. III, this implies that the system state must converge to an equilibrium in L. At any such equilibrium, $V_1 = 0$, and so $V = V_2$. If V_2 is positive definite in deviations δ_n at an equilibrium and $V_2 = 0$ by choice of constant V_o, then there exists an $\epsilon > 0$ such that $V_2 \leq \epsilon$ does not contain any other equilibria. The set of states satisfying $V \leq \epsilon$ is then positively invariant, $V_2 \leq \epsilon$ after the initial time, and the equilibrium contained in this set is asymptotically stable.

We exclude the possibility that the inequalities (58–64) are violated with equality, because this would require precise relationships between parameters that would be unlikely in practice. Then failure of these inequalities implies that not only is V_2 not positive definite at the equilibrium in question, but that there exist orientations $\hat{n}$ arbitrarily close to the equilibrium orientation $\hat{n}_o$ for which $V_2 < 0$. Beginning at this orientation with zero relative velocity ($V_1 = 0$), the state will converge to an equilibrium in which V is no larger than its initial value and $V_1 = 0$. Hence, V_2 at a convergent equilibrium is upper-bounded by its initial value. The convergent equilibrium must therefore be one of the *other* equilibria, and the equilibrium in question is unstable. This shows that the sufficient conditions for Lyapunov stability in Sec. IV (assuming that equality in the conditions is excluded) become necessary and sufficient when the damping control law (66) is applied. Stable equilibria are also then asymptotically stable.

Because Eqs. (61) and (64) cannot be satisfied (for the oblate $I_n > I_T$ mass properties assumed for the sailcraft), any equilibria that exist on the light gray line in Fig. 3 are always unstable under Eq. (66). Those on the other lines may be stable or unstable, depending on the orbit and sailcraft design parameters.

Consider specifying a spin rate ω_{no} that is larger than the largest upper limit in Eq. (31). Then there exist only two equilibria (both type I): the stability condition for type I.A (in which $\hat{n}$ aligned with $\hat{o}$ is satisfied) and the stability condition for type I.B (in which $\hat{n}$ aligned with $-\hat{o}$ is not satisfied). Therefore, type I.B equilibrium is unstable. By the center-manifold theorem [36], this equilibrium may have a stable manifold, but it has a dimension less than that of the state space $R^2 \times S^2$; hence, the set of initial states that can converge to this unstable equilibrium is thin (i.e., has measure zero in $R^2 \times S^2$). All other states converge to the stable equilibrium. Therefore, the stable type I.A equilibrium is essentially globally asymptotically stable (e.g.a.s.), implying that the sailcraft will reach this equilibrium in practice from any initial state, because any disturbance will prevent the state from remaining on a thin stable manifold leading to the unstable equilibrium.

The required spin rate can be acquired by a preliminary spin-up control law that produces torques with $\hat{n}$ components. Thereafter, only the transverse torque damping law (66) is needed to guarantee final spin with $\hat{n}$ aligned with $\hat{o}$. Similarly, $\hat{n}$ alignment along $-\hat{o}$ can be guaranteed by a suitably negative preliminary spin ω_{no}. This operational mode may be useful for initial attitude acquisition after launch vehicle separation or as a parking mode for safe, long-term, low-power operation. However, solar thrust is normal to the orbit, and no change in orbit parameters due to sail thrust can occur.

Type III.A.2 equilibria produce solar thrust in the orbit velocity direction, resulting in an increase in the orbit semimajor axis over time. For high orbits in which $\tau_{\mathrm{am}} < 3\tau_{\mathrm{gm}}$, Eq. (63) requires a small c.p.–c.m. offset for $\cos\beta > 0$ equilibria to be stable, which may be difficult to guarantee in the presence of sail shape variations. The $\cos\beta < 0$ equilibria are more robust, in that a large c.p.–c.m. offset is possible, and the required equilibrium spin can be correspondingly large in magnitude, producing more angular momentum to resist torque disturbances from sail shape variation. However, this attitude has the sailcraft normal pointed in the antisun hemisphere, requiring appropriate design of the sail reflective surface and location of solar arrays on the backside.

The type III.A.1 equilibria produce solar thrust in the antivelocity direction, reducing the semimajor axis over time. For the high orbits, slightly different equilibrium spins are required, and the stability conditions are only slightly different from those of type III.A.2. Hence, it may be difficult to ensure that the desired case is obtained from an distant initial attitude.

For lower orbits in which $\tau_{\mathrm{am}} > 3\tau_{\mathrm{gm}}$, types II.A.2 and III.A.2 equilibria are always unstable, but types II.A.1 and III.A.1 are stable for large-enough τ_{am}. This supports a reliable deorbit mode, in which $\cos\beta$ becomes smaller as τ_{am} becomes larger, producing more drag (aerobraking), and hence larger τ_{am} and smaller $\cos\beta$, eventually aligning $\hat{n}$ with the velocity vector as $\cos\beta$ goes to zero.

Figure 4 shows an example bifurcation diagram that indicates the existence and stability of equilibria based on the conditions given in Secs. III.B and IV, as a function of the inertial equilibrium spin rate ω_{no}, normalized by the orbit rate ω_o. Equilibria with black lines are stable, and those with gray lines are unstable. The + and − designations correspond to the sign of $\cos\beta$. Circle and square markers for type II equilibria correspond to those used in Fig. 3.

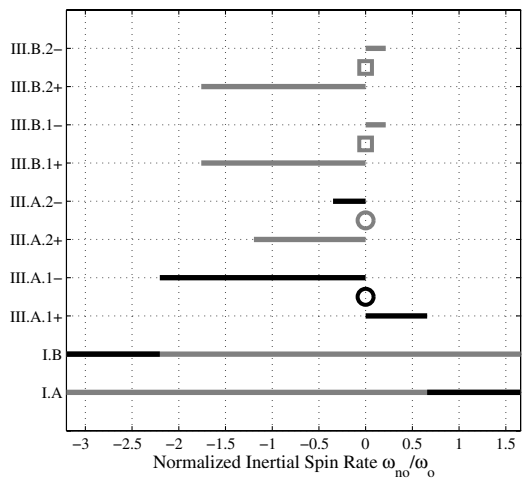

Fig. 4 Bifurcation diagram showing existence and stability of all equilibrium types as a function of the normalized inertial spin rate ω_{no}/ω_o for a particular sailcraft and orbit design. Black equilibria are stable and gray are unstable.

Sailcraft and orbit parameters used in this example are as follows. The sail is square, flat, with a 40 m^2 area, 1.7 kg mass, and a bus of 1.3 kg mass located such that the sailcraft center of mass is offset $r_c = 9.5$ cm from the sail plane along the sail normal $\hat{n}$. This stems from a design in which the sail is deployed from a 3U CubeSat [41] with a total mass of 3 kg. The sailcraft is in a 700-km-alt circular polar orbit, designed to approximate a sun-synchronous orbit with a dawn–dusk orientation of orbit nodes. This places $\hat{s}$ approximately along $\hat{o}$. Mean atmospheric density for this altitude [35] was assumed.

Note that there are only two equilibria for $\omega_{no}/\omega_o > 0.72$, corresponding to $\hat{n}$ aligned with $\hat{o}$ (type I.A, stable) and $\hat{n}$ aligned with $-\hat{o}$ (type I.B, unstable). The type I.A equilibrium is therefore e.g.a.s. Figure 5 shows how the sail normal propagates in simulation using MATLAB's ODE113 integrator.

For an orbit-rasing equilibrium (type III.A.2), with $\hat{n}$ in the sun-pointing hemisphere (e.g., $\cos\beta = 0.524$ rad), we need $\omega_n/\omega_o = -1.036$. From Fig. 4, the system has only one stable equilibrium, again making it e.g.a.s. (i.e., except for initial states on the other equilibria, a set of measure zero). Unfortunately, the desired orbit-rasing equilibrium is unstable, and the sail normal is attracted to the orbit-lowering equilibrium with $\hat{n}$ in the anti-sun-pointing hemisphere, as shown in Fig. 6.

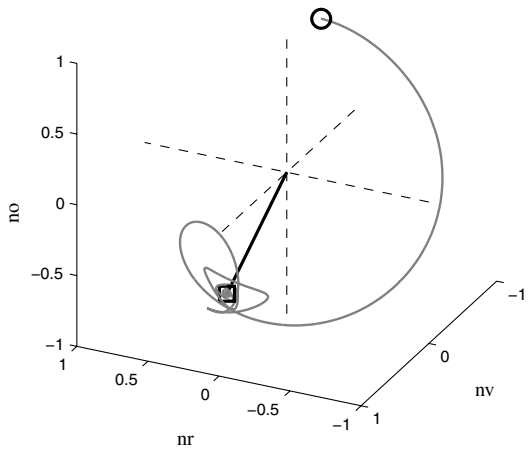

Fig. 6 Simulation of the sail normal $\hat{n}$ propagation in the LVLH frame L for beginning near an unstable type III.A.2 equilibrium, corresponding to $\omega_{no}/\omega_o = -1.036$ in Fig. 4. Simulation begins with $\hat{n}$ oriented 0.01 rad away from the unstable equilibrium at $\beta = 0.524$ and $\phi = \pi$ rad (circle) and converges to the stable equilibrium at $\beta = 2.06$ and $\phi = 0$ rad (square) in approximately 8 orbits. Damping gain $k_d = 3 \times 10^{-3}$ Nms/rad.

C. Potential Control

To stabilize an unstable equilibrium, consider adding the following control potential to V_2:

$$\Psi_c = k_p(1 - \text{sign}(\hat{n}\cdot\hat{n}_o)(\hat{n}\cdot\hat{n}_o)^2) \tag{68}$$

Following the approach in Sec. IV, the time derivative of this potential is

$$\frac{\mathrm{d}}{\mathrm{d}t}\Psi_c = -k_p{}^L\boldsymbol{\omega}_C \cdot (\hat{n}\times\hat{n}_o)|\hat{n}\cdot\hat{n}_o| \tag{69}$$

and this must be added to the $\dot{V}_b$ found earlier, resulting in a nonzero $\dot{V}$. However, adding a second control torque

$$\boldsymbol{\tau}_{c2} = k_p(\hat{n}\times\hat{n}_o)|\hat{n}\cdot\hat{n}_o| \tag{70}$$

in Eq. (50) produces a new term in $\dot{V}_a$ that cancels with the new term (69) in $\dot{V}_b$, preserving $\dot{V} = 0$ in Eq. (67). The same LaSalle arguments for stability still apply, but the positive-definiteness of V_2 about the equilibrium orientation $\hat{n}_o$ is now strengthened by the additional stiffness produced by the control potential Ψ_c. In particular, carrying out the deviation analysis as in Sec. IV results in an additional k_p term added to the left-hand side of all the stability conditions in Sec. IV. Thus, a large-enough (positive) k_p exists, via a large-enough control gain k_p in Eq. (70), to cause V_2 to be positive definite at any of the equilibria in L, yielding asymptotic stability in conjunction with Eq. (66). The stability conditions can also be used to find the minimum potential gain to stabilize a given equilibrium (e.g., to minimize requirements on control actuators). This stiffness control law effectively produces torques in response to errors in the cone β and clock ϕ angles relative to the desired equilibrium orientation. Figure 7 shows how this can stabilize the desired orbit-rasing equilibrium discussed earlier.

Note that the additional control torque $\boldsymbol{\tau}_{c2}$ in Eq. (70) is zero at the equilibrium attitude ($\hat{n} = \hat{n}_o$), and so this additional control stiffness does not upset the conditions for equilibrium spin ω_{so} from Sec. III for a given desired equilibrium orientation (β_o and ϕ_o). However, it does change the equilibrium equation at other orientations; that is, it may be able to eliminate (or create) other equilibria.

D. Control Robustness

In this section, we consider various nonideal conditions and their effects on equilibrium location and stability. First, if a desired inertial spin rate ω_{no} is selected on a boundary of the interval of existence [Eq. (31)], then errors in achieving $\omega_n = \omega_{no}$ or uncertainties in the

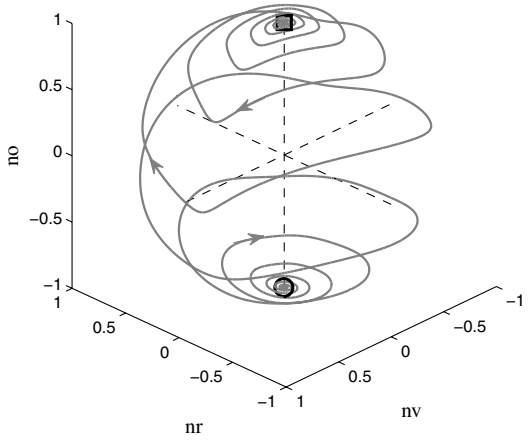

Fig. 5 Simulation of the sail normal $\hat{n}$ propagation in the LVLH frame L for an essentially globally asymptotically stable type I.A equilibrium, corresponding to $\omega_{no}/\omega_o = 1.5$ in Fig. 4. Simulation begins with $\hat{n}$ oriented 0.001 rad away from the unstable equilibrium at $\beta = \pi$ rad (circle) and converges to the equilibrium at $\beta = 0$ (square) in approximately 14 orbits. Damping gain $k_d = 3 \times 10^{-3}$ Nms/rad.

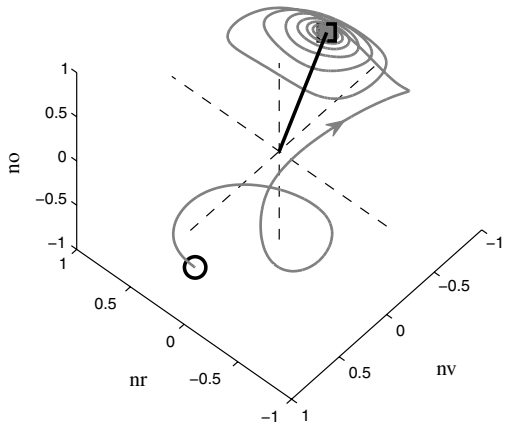

Fig. 7 Simulation of the sail normal $\hat{n}$ propagation in the LVLH frame L using a control potential in addition to damping, for $\hat{n}$ beginning near the (formerly stable) type III.A.1 equilibrium in Fig. 6 (circle). The orbit-raising equilibrium is now stable, and $\hat{n}$ converges to $\beta = 0.524$ and $\phi = \pi$ rad (square) in approximately 5 orbits. Damping gain $k_d = 3 \times 10^{-3}$ Nms/rad and the potential gain $k_p = 1 \times 10^{-4}$ Nm/rad.

parameters $\tau_{am}, \tau_{sm}, \omega_o, I_n$, or I_T can cause the equilibrium of interest to vanish. Otherwise, equilibrium location is a continuous function of the spin rate and the parameters. Stability of types II or III equilibria is not a function of ω_n, but is a function of the parameters. Stability of type I is also a function of ω_n, however, and so ω_{no} must be selected away from the stability boundaries to obtain robust stability of (one of) these two equilibria.

If the orbit normal $\hat{o}$ is not aligned with the sailcraft-to-sun vector $\hat{s}$, then $\hat{s}$ cones in the L frame at orbit rates, causing a periodic torque that eliminates equilibria in the L frame. However, the strong attraction to a desired orientation $\hat{n}_o$ in L due to the stiffness and damping control laws makes the system robust to this perturbation torque. Similarly, specifying a desired inertial spin rate ω_{no} that is incorrect for the parameters $\tau_{am}, \tau_{sm}, \omega_o, I_n$, or I_T causes the desired orientation $\hat{n}_o$ in L to no longer be at an equilibrium. The control law provides continuous torque to offset this disturbance from $\hat{n}_o$ pointing. Figure 8 shows the case of Fig. 7 with a large orbit precession (40 deg in right ascension) of $\hat{o}$ away from sun pointing and a desired spin rate ω_{no} that is 50% too large. The resulting pointing error has an offset of approximately 4 deg and an orbit-periodic ripple of less than 2 deg, demonstrating very good robustness to these large perturbations. The control torques in this case dominate the environmental torques.

If the orbit misalignment is reduced to 10 deg and the potential gain is reduced to 2×10^{-5}, with an initial condition at a cone angle of zero (e.g., when transitioning from a type I parking mode), we see that environmental torques dominate at steady state, greatly reducing the requirements on actuator torque magnitude (Fig. 9).

The control torques τ_{c1} and τ_{c2} may introduce errors due to inaccurate sensing or inaccurate actuation. Actuation using sail c.p.–c.m. offset is perhaps the greatest source of error due to uncertainties in sail shape. Robustness to this error was investigated by introducing a misalignment of the control torque in the body frame. Figure 10 shows the effects of a 6 deg rotation of torque in the transverse plane and a 6 deg tilting of the torque away from the sail normal in C frame coordinates. The case has the same conditions as Fig. 8, except the damping gain has been increased to 5×10^{-3} Nms/rad. The system is sensitive to torque misalignments at low damping gains because the contraction effect is small. In this case, a steady-state orbit-periodic ripple in orientation error exists with an amplitude of approximately 10 deg peak–peak. Larger damping gains reduce this ripple. Figure 11 shows the environmental and control torques for this case.

Note that in the case of large perturbations, the control torques once again dominate the environmental torques, and a steady-state torque ripple occurs due to both orbit misalignment and body-frame control-torque errors. Despite the large disturbances, a strong-enough attraction to the equilibrium occurs to maintain reasonable

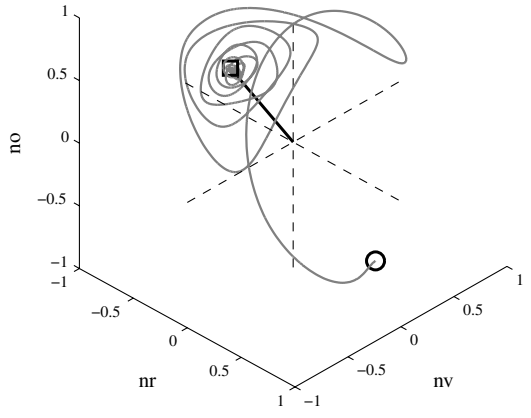

Fig. 8 Propagation of $\hat{n}$ in the LVLH frame L using the same control gains as in Fig. 7, but with $\hat{o}$ precessed 40 deg away from $\hat{s}$, and with a desired inertial spin rate ω_n that is 50% too large. The view in the L frame is reversed for clarity, and a different initial condition is also shown. Motion converges to the close vicinity of the desired orbit-raising attitude in about 4 orbits.

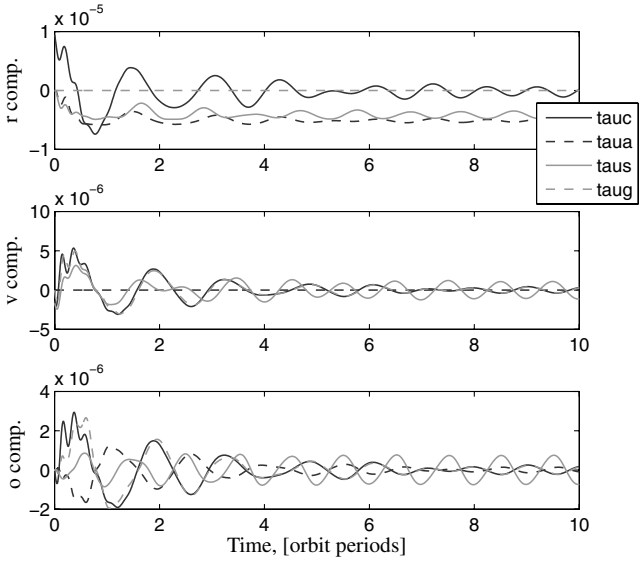

Fig. 9 Control and environmental torques (Nm) for a case of mild disturbances (10 deg misalignment of $\hat{s}$ relative to $\hat{o}$) and an initial cone angle error of 30 deg, with potential gain $k_p = 2 \times 10^{-5}$ Nm/rad.

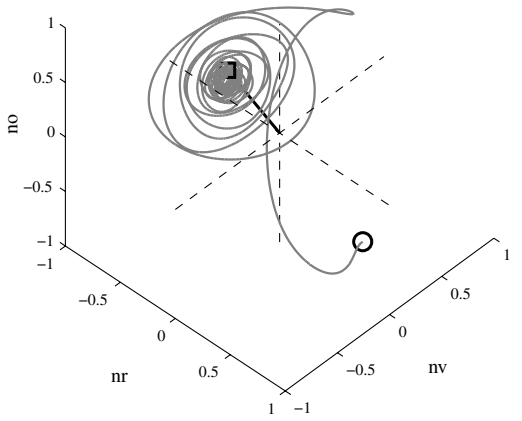

Fig. 10 Propagation of $\hat{n}$ in the LVLH frame L using the same conditions as in Fig. 7, but torque misalignments and a larger damping gain of 5×10^{-3} Nms/rad. Motion converges to the close vicinity of the desired orbit-raising attitude in about 2 orbits.

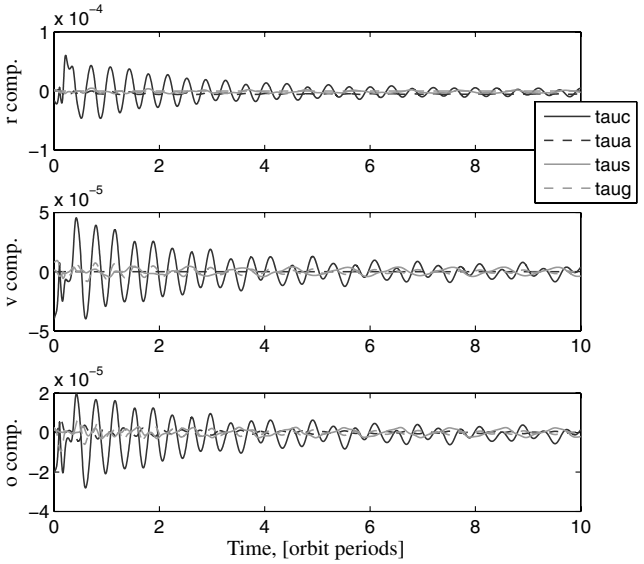

Fig. 11 Control and environmental torques (Nm) for the case shown in Fig. 10.

pointing of $\hat{n}$ to produce orbit-raising solar thrust. Also, the dominant frequency content of these torques is less than 5×10^{-4} Hz (periods greater than a one-third orbit), which is likely to be more than 1 order of magnitude below the lowest structural resonance mode frequency, mitigating concerns about control–structure interaction.

VI. Conclusions

Solar sail propulsion enables a large class of missions for both large and small spacecraft. For small-satellite applications, mass associated with attitude control is an especially significant factor in the system design. Whereas conventional control systems are typically sized to reject the environmental disturbances such as aerodynamic torques and gravity-gradient torques, these torques can be much larger for solar sails, due to the large area-to-mass ratio for which they are designed. Mass-efficient attitude control does not have the capability to oppose these large torques over reasonable spacecraft lifetimes. This paper has shown that these environmental torques can be fortuitously employed, together with appropriate spin dynamics, such that thrust-vector pointing control can be achieved for a virtually unlimited duration.

This capability relies on operating the sailcraft near equilibrium points at which environmental torques balance momentum precession. The complete set of pointing equilibria in the local-vertical/local-horizontal frame was described, along with their use in various sailcraft operational modes of interest and their dependence of their existence on orbit and sailcraft parameters. Conditions for Lyapunov stability of these equilibria were also derived. The addition of a particular type of damping control produces asymptotic stability and corresponding necessary and sufficient conditions on the system parameters. The addition of a control potential was shown to provide orientation stiffness that can stabilize any of these equilibrium points.

This control approach was also shown to be robust against several likely imperfections in sailcraft operation: coning of the sun vector in LVLH, inaccurate balance between environmental torques and momentum precession, and misaligned control-torque vectors due to sail shape uncertainty. Other nonidealities such as elliptic orbits and the use of magnetic control torque will be investigated in a subsequent paper.

Knowledge of possible equilibria and their stability properties provides useful data for mission and sailcraft design. The corresponding control theory also enables rational decisions concerning the need for active control and provides a means to estimate the required actuator and sensor requirements.

Acknowledgment

Support for this work was provided by NASA Marshall Space Flight Center, NNX07AO89G, and is gratefully acknowledged.

References

[1] Wright, J. L., *Space Sailing*, Gordon and Breach, Philadelphia, 1992, Chap. 2.

[2] McInnes, C. R., *Solar Sailing: Technology, Dynamics, and Mission Applications*, Springer Praxis, New York, 1999, pp. 19–25, 47–50.

[3] Lisano, M., Lawrence, D., and Piggott, S., "Solar Sail Transfer Trajectory Design and Stationkeeping Control for Missions to the Sub-L1 Equilibrium Region," AAS/AIAA Space Flight Mechanics Meeting, Copper Mountain, CO, American Astronautical Society Paper 05-219, Jan. 2005.

[4] Wie, B., "Solar Sail Attitude Control and Dynamics, Part 1," *Journal of Guidance, Control, and Dynamics*, Vol. 27, No. 4, 2004, pp. 526–535. doi:10.2514/1.11134

[5] Lappas, V., Wokes, S., Leipold, M., Lyngvi, A., and Falkner, P., "Guidance and Control for an Interstellar Heliopause Probe (IHP) Solar Sail Mission to 200 AU," AIAA Guidance, Navigation, and Control Conference, San Francisco, AIAA Paper 2005-6085, Aug. 2005.

[6] Lappas, V., Wie, B., McInnes, C., Tarabini, L., Gomes, L., and Wallace, K., "Microsolar Sails for Earth Magnetotail Monitoring," *Journal of Spacecraft and Rockets*, Vol. 44, No. 4, 2007, pp. 840–848. doi:10.2514/1.23456

[7] Wie, B., and Murphy, D., "Solar-Sail Attitude Control Design for a Sail Flight Validation Mission," *Journal of Spacecraft and Rockets*, Vol. 44, No. 4, 2007, pp. 809–821. doi:10.2514/1.22996

[8] Wie, B., "Solar Sail Attitude Control and Dynamics, Part 2," *Journal of Guidance, Control, and Dynamics*, Vol. 27, No. 4, 2004, pp. 536–544. doi:10.2514/1.11133

[9] Van der Ha, J. C., and Modi, V. J., "Orbital Perturbations and Control by Solar Radiation Forces," *Journal of Spacecraft and Rockets*, Vol. 15, No. 2, 1978, pp. 105–112. doi:10.2514/3.57293

[10] Garwin, R. L., "Solar Sailing—A Practical Method of Propulsion Within the Solar System," *Jet Propulsion*, Vol. 28, Mar. 1958, pp. 188–190.

[11] Sands, N., "Escape from Planetary Gravitational Fields by Use of Solar Sails," *Journal of the American Rocket Society*, Apr. 1961, pp. 527–531.

[12] Fimple, W. R., "Generalized Three-Dimensional Trajectory Analysis of Planetary Escape by Solar Sail," *Journal of the American Rocket Society*, Vol. 32, June 1962, pp. 883–887.

[13] Coulter, D., "A Brief History of Solar Sails," *Science@NASA Headline News*, 31 July 2008, http://science.nasa.gov/headlines/y2008/31jul_solarsails.htm, [retrieved 14 Dec. 2008].

[14] Rios-Reyes, L., and Scheeres, D. J., "Solar Sail Navigation: Estimation of Force, Moments, and Optical Parameters," *Journal of Guidance, Control, and Dynamics*, Vol. 30, No. 3, 2007, pp. 660–668. doi:10.2514/1.24340

[15] Bladt, J. J., Lawrence, D. A., and L. M. Ward, "Solar Sail Attitude Control Sensitivity to Solar Radiation Pressure Model Accuracy," AAS/AIAA Space Flight Mechanics Conference, Maui, HI, American Astronautical Society Paper 04-282, Feb. 2004.

[16] Sakamoto, H., Park, K. C., and Miyazaki, Y., "Effect of Static and Dynamic Solar Sail Deformation on Center of Pressure and Thrust Forces," AIAA Guidance, Navigation, and Control Conference, Keystone, CO, AIAA Paper 2006-6184, Aug. 2006.

[17] Thompson, W. T., "Spin Stabilization of Attitude Against Gravity Torque," *Journal of the Astronautical Sciences*, Vol. 9, No. 1, 1962, pp. 31–33.

[18] Pringle, R., "Bounds on the Libration of a Symmetrical Satellite," *AIAA Journal*, Vol. 2, No. 5, 1964, pp. 908–912. doi:10.2514/3.2436

[19] Likins, P. W., "Stability of a Symmetrical Satellite in Attitudes Fixed in an Orbiting Reference Frame," *Journal of the Astronautical Sciences*, Vol. 12, No. 1, 1965, pp. 18–24.

[20] Roberson, R. E., "Two Decades of Spacecraft Attitude Control," *Journal of Guidance and Control*, Vol. 2, No. 1, 1979, pp. 3–8. doi:10.2514/3.55824

[21] Hughes, P. C., *Spacecraft Attitude Dynamics*, Wiley, New York, 1986, pp. 232–264, 354–382.

[22] Modi, V. J., and Shrivastava, S. K., "Satellite Attitude Dynamics and Control in Presence of Environmental Torques—A Survey," AIAA/AAS Astrodynamics Conference, San Diego, CA, AIAA Paper 82-1414, Aug. 1982.

[23] Modi, V. J., and Shrivastava, S. K., "Optimized Performance of a Semipassive Aerodynamic Controller," *AIAA Journal*, Vol. 11, No. 8, 1973, pp. 1080–1085. doi:10.2514/3.50556

[24] Chen, Y.-H., Hong, Z.-C., and Lin, C.-H., "Aerodynamic and Gravity Gradient Stabilization for Microsatellites," *Acta Astronautica*, Vol. 46, No. 7, 2000, pp. 491–499. doi:10.1016/S0094-5765(99)00191-5

[25] Modi, V. J., and Kumar, K., "Attitude Control of Satellites Using the Solar Radiation Pressure," *Journal of Spacecraft and Rockets*, Vol. 9, No. 9, 1972, pp. 711–713. doi:10.2514/3.61784

[26] Modi, V. J., and Pande, K. C., "On the Periodic Solutions and Resonance of Spinning Satellites in Near-Circular Orbits," *Celestial Mechanics*, Vol. 11, No. 2, 1975, pp. 195–221. doi:10.1007/BF01230545

[27] Modi, V. J., and Pande, K. C., "Aerodynamic-Solar Hybrid Attitude Control of Near-Earth Satellites," *Journal of the Astronautical Sciences*, Vol. 22, July–Sept. 1974, pp. 36–45.

[28] Swartwout, M. A., "Earth Escape Using a Slowly Rotating, Doubly Reflective Solar Sail," *Journal of Guidance, Control, and Dynamics*, Vol. 28, No. 2, 2005, pp. 374–377. doi:10.2514/1.12687

[29] Lawrence, D. A., Irwin, T. J., and Whorton, M. S., "Solar Sail Thrust Measurement During Coning Operations," AIAA Guidance, Navigation, and Control Conference, Keystone, CO, Aug. 2006, AIAA Paper 2006-6183.

[30] Rios-Reyes, L., and Scheeres, D., "Robust Solar Sail Trajectory Control for Large Pre-Launch Modeling Errors," AIAA Guidance, Navigation, and Control Conference, San Francisco, AIAA Paper 2005-6173, Aug. 2005.

[31] Lawrence, D. A., and Piggott, S., "Integrated Trajectory and Attitude Control for a Four-Vane Solar Sail," AIAA Guidance, Navigation, and Control Conference, San Francisco, AIAA Paper 2005-6082, Aug. 2005.

[32] Kane, T. R., and Levinson, D. A., *Dynamics, Theory and Applications*, McGraw–Hill, New York, 1985, pp. 66-70, 370.

[33] Nakano, T., "A Study on the Stability of Spinning Solar Sailcraft with Huge Membrane," 56th International Astronautical Congress of the IAF, Fukuoka, Japan, International Aeronautical Federation Paper IAC-05-A.4.01, Oct. 2005.

[34] Rotunno, M., Basso, M., Pome, A. B., and Sallusti, M., "A Comparison of Robust Attitude Control Techniques for a Solar Sail Spacecraft," AIAA Guidance, Navigation, and Control Conference, San Francisco, AIAA Paper 2005-6083, Aug. 2005.

[35] Wertz, J. R. (ed.), *Spacecraft Attitude Determination and Control*, Kluwer Academic, Dordrecht, The Netherlands, 1978, pp. 566–574, 820.

[36] Guckenheimer, J., and Holmes, P., *Nonlinear Oscillations, Dynamical Systems, and Bifurcations of Vector Fields*, Springer–Verlag, New York, 1983, pp. 13–14, 127.

[37] Khalil, H. K., *Nonlinear Systems*, 3rd ed., Prentice–Hall, Upper Saddle River, NJ, 2002, pp. 114, 128.

[38] Blomquist, R., "Solar Blade Nanosatellite Development–Heliogyro Development, Dynamics, and Control," 13th AIAA/USU Conference on Small Satellites, Logan, UT, Utah State Univ. Paper SSC99-VII-3, Aug. 1999.

[39] Lawrence, D. A., and Piggott, S., "Solar Sailing Trajectory Control for Sub-L1 Stationkeeping," AIAA Guidance, Navigation, and Control Conference, Providence, RI, AIAA Paper 2004-5014, Aug. 2004.

[40] Bladt, J. J., and Lawrence, D. A., "Solar Sail Attitude Control Performance Comparison," AAS Guidance and Control Conference, Breckenridge, CO, American Astronautical Society Paper 05-003, Feb. 2005.

[41] Lan, W., Brown, J., Torrian, A., Coelho, R., Brooks, L., and Suari, J. P., "CubeSat Development in Education and into Industry," SPACE 2006, San Jose, CA, AIAA Paper 2006-7296, Sept. 2006.